

The Lyman- α glow of gas falling into the dark matter halo of a $z = 3$ galaxy

M. Weidinger^{1,2}, P. Møller¹, J. P. U. Fynbo^{2,3}

¹ European Southern Observatory, Karl-Schwarzschild-Straße 2, D-85748 Garching bei München, Germany

² Institute of Physics and Astronomy, University of Aarhus, Ny Munkegade, DK-8000 Århus C, Denmark

³ Astronomical Observatory, University of Copenhagen, Juliane Maries Vej 30, DK-2100 Copenhagen Ø, Denmark

Quasars are the visible signatures of super-massive black holes in the centres of distant galaxies. It has been suggested¹ that quasars are formed during “major merger events” when two massive galaxies collide and merge, leading to the prediction that quasars should be found in the centres of the regions of largest overdensity in the early Universe. In dark matter (DM)-dominated models of the early Universe, massive DM halos are predicted to attract the surrounding gas, which falls towards its centre. The neutral gas is not detectable in emission by itself, but gas falling into the ionizing cone of such a quasar will glow in the Lyman- α line of hydrogen, effectively imaging the DM halo². Here we present a Ly α image of a DM halo at redshift 3, along with a two-dimensional spectrum of the gaseous halo. Our observations are best understood in the context of the standard model for DM halos³; we infer a mass of $(2 - 7) \times 10^{12}$ solar masses (M_{\odot}) for the halo.

Using radiative transfer calculations, Haiman & Rees^{ref2} predicted that gas falling into a DM halo between redshifts 3 and 8 that was harbouring a quasar should be detectable in Ly α -emission at flux levels accessible to present day telescopes, owing to the reprocessing of quasar ultraviolet photons. Recently, Barkana & Loeb⁴ found absorption features in quasar spectra, which they interpreted as a signature of neutral hydrogen (HI) falling into the DM halos surrounding two quasars. Such absorption features can be used to study the gas in one dimension (1D) along the line of sight, whereas detection of extended Ly α -emission can be used in a 2D study, providing more constraints on the interplay between gas, quasar radiation and DM halo.

In a deep Ly α narrow-band image we detected asymmetric extended emission North-East of the $z = 3$ radio-quiet quasar Q1205-30, making this quasar a prime candidate for a study of its DM halo. The extended Ly α emission was first thought to be related to a foreground absorber⁵, but deep follow-up spectroscopy obtained with the FORS1 instrument on the ESO Very Large Telescope allowed us to measure precise redshifts of quasar, absorber, and extended emission, clearly linking the extended emission to the quasar, not the absorber. The 2D spectrum is presented in Fig. 1 (details of the data reduc-

tion will be presented elsewhere). In the 2D spectrum the wavelength increases along the abscissa, and the position on the sky changes along the ordinate. In order to reveal the underlying extended emission we have optimally extracted the 2D quasar spectrum by fitting and removing the quasar spectral point-spread function⁶. Spectroscopic detection of kinematically resolved extended Ly α -emission is not uncommon^{7,8}, but it does not provide sufficient information to distinguish between scenarios of – for example – nearly edge-on disks and gaseous halos. For this, morphological information is needed. In Fig. 2a we present a 10×10 arcsec² narrow-band image of the extended emission.

A quasar emits its radiation in an ionizing cone with an opening angle of Ψ , while we observe the whole system under an inclination angle of θ (see Fig. 3). The surface brightness at each point in the vicinity of the quasar is calculated by integration of the volume emission along the line of sight⁹. We take the gas density profile to be a power-law, $n_{\text{HI}}(r) = n_{\text{HI},1} (r/1 \text{ kpc})^{-\alpha}$, with a slope α and a neutral hydrogen density at a distance of 1 kpc $n_{\text{HI},1}$, because this appears in numerical simulations of DM halos to be a good approximation at small radii¹⁰. If we assume a mass of the DM halo, we may calculate the observed infall velocity in the model. At a given projected distance from the quasar the observed velocity is the average projected velocity weighted with the emissivity of the gas along the line of sight.

Applying this model to Q1205-30, our calculation shows that the Ly α halo should be detectable with 8-m class telescopes up to several arcsec from the quasar, assuming a modest amount of neutral hydrogen infall. Considering – for now – the case where only one cone is visible, the extended emission may be symmetric (if $\theta \approx 0$, that is, the cone is seen close to end-on) or highly asymmetric (if $\theta \approx \Psi/2$). By fitting the calculated surface brightness maps to the observed narrow-band image we establish a relation between the opening angle and the best-fitting inclination angle. Thus, we are left with the opening angle, Ψ , the slope, α , and the neutral hydrogen density at 1 kpc, $n_{\text{HI},1}$, as the only free parameters of the model. In Fig. 2, we compare our observed narrow-band image to calculated Ly α surface brightness maps with an opening angle $\Psi = 110^\circ$ and three different inclination

angles: the best-fit and two others. For the expected large opening angles ($\Psi \approx 90^\circ - 120^\circ$)^{11,12}, varying the opening angle primarily affects the shape of the surface brightness profile seen on the side where the emission is weakest (in Fig. 3, that would be on side A of the sightline), and only has a minor effect on the shape of the main emission profile (on side B). The gas density scale, $n_{\text{HI},1}$, determines the normalization of the surface brightness profile, but not the shape, which is set by the slope α . The results are not dependent on the choice of a power-law gas density profile. An exponential gas density profile provides an equally good fit to the data.

The extended emission is spatially resolved, so we can measure its surface brightness profile and velocity profile (see Fig. 4). The surface brightness profile is measured by integrating the flux from 4900 Å to 4947 Å in each spatial bin. The velocity in each spatial bin is measured by fitting a gaussian to the line profile. The infall velocity is calculated relative to the redshift $z = 3.041$ of the quasar.

We find that the model describes the observations well. The opening angle is the only parameter which remains unconstrained, so we plot the surface brightness profile for a range of opening angles (Fig. 4a). The best-fit values for the neutral hydrogen density at 1 kpc vary less than a factor two between $\Psi = 90^\circ$ and 170° , while the slope varies between 0.02 and 0.09. The velocity profile of the extended emission (Fig. 4b) arises as a projection effect, and fitting velocity curves of canonical DM halo profiles^{ref3} to the observed velocities, we infer a virial mass of $(2 - 7) \times 10^{12} M_\odot$ for the DM halo. An identical mass estimate is obtained when using an exponential gas density profile. The HI density from our best fitting model allows us to calculate an accretion rate of $\sim 0.1 M_\odot \text{yr}^{-1}$ in neutral hydrogen. The total accretion rate will be higher as the gas is highly ionized.

Where studies based only on spectra are unable to provide evidence to distinguish between several different scenarios, the combination of deep imaging and deep spectroscopy allows us to rule out alternative explanations of the extended emission. Jets are generally believed to be present in radio-quiet quasars and are predicted to extend out to $\sim 0.1 \text{ kpc}$ ¹³, where the extended Ly α emission around Q1205-30 extends out to $\sim 30 \text{ kpc}$. Outflowing galactic winds are believed to be triggered by supernovae going off inside the galaxy, and are therefore expected to be metal-enriched. Our detection limit of $4 \times 10^{-18} \text{ erg s}^{-1} \text{ cm}^{-2} \text{ arcsec}^{-2}$ (3σ) ensures that we are able to detect the CIV and HeII lines typical in extended emission around radio-loud quasars¹⁴. We did not detect any of these lines, so the gas appears not to have been enriched by supernovae.

Received 24 March; accepted 28 June 2004.

Notes

¹e.g. Carlberg, R.G. Quasar evolution via galaxy mergers. *Astrophys. J.* **350**, 505-511 (1990)

²Haiman, Z. & Rees, M. Extended Ly α Emission around Young Quasars: A Constraint on Galaxy Formation. *Astrophys. J.* **556**, 87-92

(2001)

³Navarro, J.F., Frenk, C.S., & White, S.D.M. A Universal Density Profile from Hierarchical Clustering. *Astrophys. J.* **490**, 493-508 (1997)

⁴Barkana, R. & Loeb, A. Spectral signature of cosmological infall of gas around the first quasars. *Nature* **421**, 341-343 (2003)

⁵Fynbo, J.P.U., Thomsen, B., & Møller, P. Ly α emission from a Lyman limit absorber at $z=3.036$. *Astron. Astrophys.* **353**, 457-464 (2000)

⁶Møller, P. Spectral PSF Subtraction I: The SPSF Look-Up-Table Method. *The ESO Messenger* **99**, 31-33 (2000)

⁷Møller, P., Warren, S.J., Fall, S.M., Jakobsen, P., & Fynbo, J.U. SPSF Subtraction II: The Extended Ly α Emission of a Radio Quiet QSO. *The ESO Messenger* **99**, 33-35 (2000)

⁸Bunker A., Smith, J., Spinrad, H., Stern, D., & Warren, S.J. Illuminating Protogalaxies? The Discovery of Extended Lyman- α Emission around a QSO at $z = 4.5$. *Astrophys. Sp. Sci.* **284**, 357-360 (2003)

⁹Gould, A. & Weinberg, D.H. Imaging the Forest of Lyman Limit Systems. *Astrophys. J.* **468**, 462-468 (1996)

¹⁰Barkana, R. A model for infall around virialized haloes. *Mon. Not. R. Astron. Soc.* **347**, 59-66 (2004)

¹¹Lawrence, A. The relative frequency of broad-lined and narrow-lined active galactic nuclei - Implications for unified schemes. *Mon. Not. R. Astron. Soc.* **252**, 586-592 (1991)

¹²Elvis, M. A Structure for Quasars. *Astrophys. J.* **545**, 63-76 (2000)

¹³Blundell, K.M., Beasley, A.J., & Bicknell, G.V. A Relativistic jet in the radio-quiet quasar PG 1407+263. *Astrophys. J.* **591**, L103-106 (2003)

¹⁴Heckman, T.M., Lehnert, M.D., Miley, G.K., & van Breugel, W. Spectroscopy of spatially extended material around high-redshift radio-loud quasars. *Astrophys. J.* **381**, 373-385 (1991)

Correspondence and requests for materials should be addressed to M.W. (mweiding@eso.org).

Acknowledgements Based on observations made with ESO Telescopes at the Paranal Observatory.

Competing interests statement. The authors declare that they have no competing financial interests.

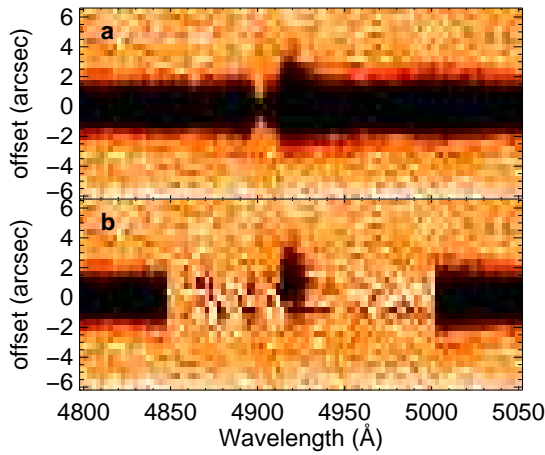


Figure 1: Two-dimensional spectrum of Q1205-30 and the extended Ly α emission. The wavelength increases along the abscissa, the position on the sky changes along the ordinate. The spectroscopy was performed with a slit position angle of 7.9° east of north (see Fig. 2a). **a**, The 2D quasar spectrum. The extended Ly α emission is faintly visible at $4,920 \text{ \AA}$. **b**, The quasar spectrum has been subtracted between the wavelengths $4,850 - 5,000 \text{ \AA}$, clearly revealing the underlying extended emission.

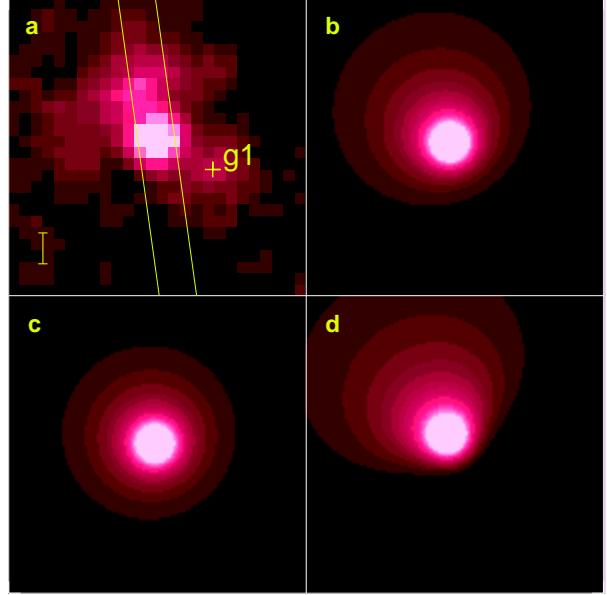


Figure 2: Narrow-band image of the extended Ly α emission compared to models. **a**, Image of the $10 \times 10 \text{ arcsec}^2$ region around Q1205-30 seen in Ly α . The quasar has been subtracted from this image to reveal the underlying extended emission. A 1.2-arcsec -wide slit is overplotted at a position angle of 7.9° east of north, and the position of an unrelated foreground galaxy⁵ is marked g1. The vertical bar on the lower left is 1 arcsec high. **b – d**, Calculated $10 \times 10 \text{ arcsec}^2$ surface brightness maps for an opening angle of $\Psi = 110^\circ$ and three inclination angles. The best fitting inclination angle ($\theta = 27^\circ$) is shown in **b**, two other inclination angles are shown in **c** ($\theta = 10^\circ$, excluded at 3.5σ) and **d** ($\theta = 50^\circ$, excluded at 3σ) for comparison. Given an opening angle, the best-fit inclination angle is determined in the following way. An average surface brightness profile, parallel and perpendicular to the apparent major axis of the extended emission, is fitted to the same average calculated from the models. For each opening angle Ψ the best-fitting inclination angle is found.

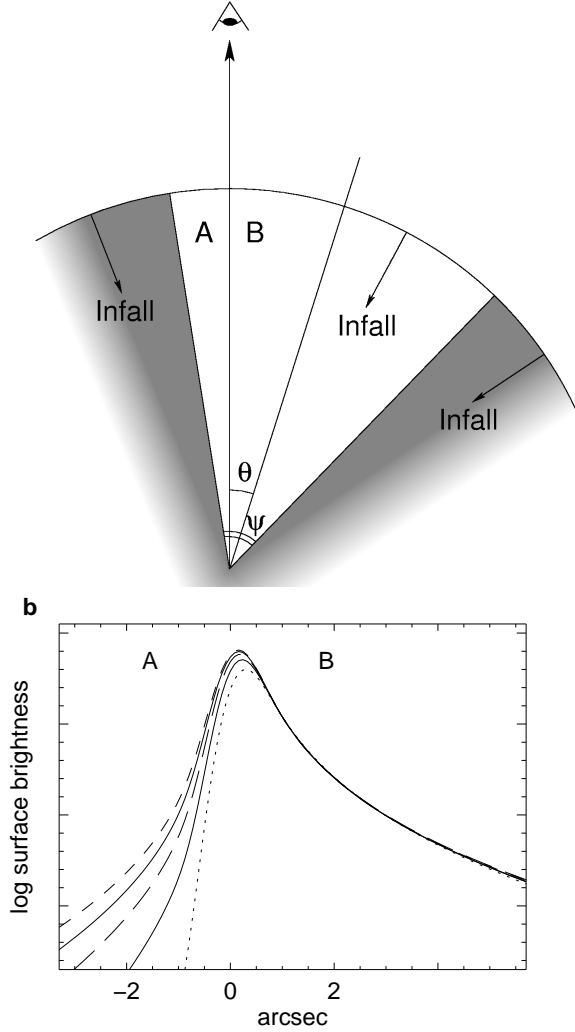


Figure 3: Schematic presentation of the model. **a**, A quasar is located in the centre of a DM halo into which neutral hydrogen is falling. The ionizing photons from the quasar are emitted in a cone of opening angle Ψ , and they cause the infalling HI to glow in Ly α . The observer views the system inclined at an angle θ . The surface brightness at each point is calculated by integration of the volume emission along the line of sight^{ref9}: $\Sigma_{\text{Ly}\alpha} = \frac{\int E_{\text{Ly}\alpha} \dot{n}_{\text{Ly}\alpha}(r) dl}{4\pi D_L^2} \frac{D_A^2}{d\Omega}$, where $E_{\text{Ly}\alpha} = 10.4$ eV is the energy of a Ly α photon, $\dot{n}_{\text{Ly}\alpha}(r)$ is the production rate of Ly α photons at a distance r from the quasar, D_L is the quasar luminosity distance, and D_A is the angular distance, such that $\frac{d\Omega}{D_A^2}$ is the conversion from cm^2 to arcsec^2 . The Ly α production rate is $\dot{n}_{\text{Ly}\alpha}(r) = \eta_{\text{thin}} n_{\text{HI}}(r) \Gamma(r)$, and $\eta_{\text{thin}} = 0.42$ is the probability for an ionizing photon to result in a Ly α photon in the optically thin case, $n_{\text{HI}}(r)$ is the volume density of neutral hydrogen atoms, and $\Gamma(r)$ is the ionization rate of hydrogen atoms. **b**, A schematic illustration of the predicted surface brightness profile for various opening angles $\Psi = 90^\circ$ (dotted), 110° (solid), 130° (long-dashed), 150° (solid), and 170° (short-dashed), and a fixed inclination angle $\theta = 40^\circ$. The profiles are presented as they would appear when observed with a seeing of 0.7 arcsec through a slit aligned with the line between the sightline l and the symmetry axis of the cone. Negative angular distances correspond to emission seen from side A, and positive angular distances correspond to emission seen from side B.

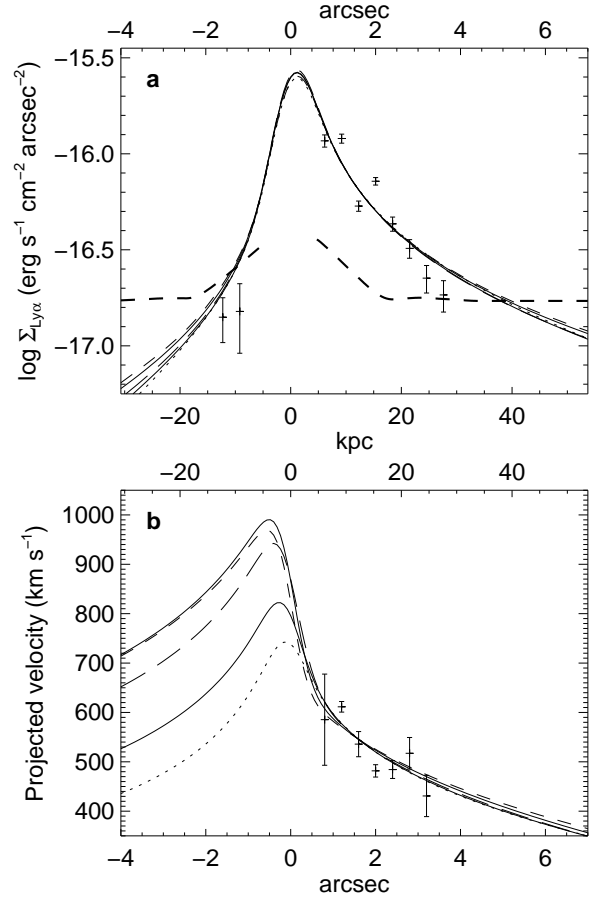


Figure 4: Calculated surface brightness profile and projected velocity. **a**, Comparison of the calculated and observed surface brightness profile. Thin lines are the calculated profile for various opening angles, and data points are our observations of the extended Ly α -emission around Q1205-30. The calculations were performed for opening angles and inclination angles of $\Psi = 90^\circ, \theta = 22.5^\circ$ (dotted), $\Psi = 110^\circ, \theta = 27.2^\circ$ (solid), $\Psi = 130^\circ, \theta = 31.8^\circ$ (long-dashed), $\Psi = 150^\circ, \theta = 36.5^\circ$ (solid), and $\Psi = 170^\circ, \theta = 41.1^\circ$ (short-dashed). The thick dashed line shows our 5σ detection limit. **b**, Comparison of calculated and observed projected velocity relative to the quasar redshift. Lines are the calculated best-fit velocity profiles for opening angles and inclination angles of $\Psi = 90^\circ, \theta = 22.5^\circ$ (dotted), $\Psi = 110^\circ, \theta = 27.2^\circ$ (solid), $\Psi = 130^\circ, \theta = 31.8^\circ$ (long-dashed), $\Psi = 150^\circ, \theta = 36.5^\circ$ (solid), and $\Psi = 170^\circ, \theta = 41.1^\circ$ (short-dashed). Three of the measurements in panel **a** were too faint to allow a secure velocity determination. In both panels the angular distance was converted to physical distance assuming a flat $\Omega_\Lambda = 0.7$ Universe with a Hubble constant $H_0 = 70 \text{ km s}^{-1} \text{ Mpc}^{-1}$. Error bars are 1σ .